

A Novel IGBT Inverter Module for Low-Power Drive Applications

By M.K Kim, K.Y Jang, B.H Choo, J.B Lee, B.S Suh, T.H Kim

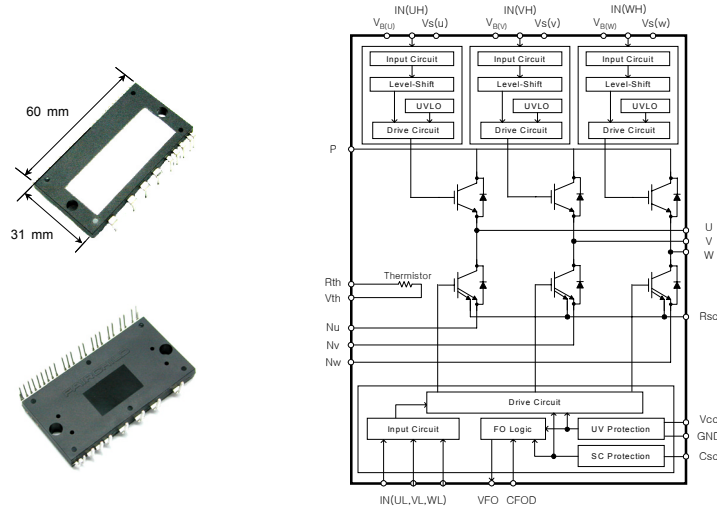
Abstract - This paper presents a novel 3-phase IGBT module called the SPM (Smart Power Module). This is a new design developed to provide a very compact, low cost, high performance and reliable motor drive system. Several distinct design concepts were used to achieve the highly integrated functionality in a new cost-effective small package. An overall description to the SPM is given and actual application issues such as electrical characteristics, circuit configurations, thermal performance and power ratings are discussed.

I. Introduction

The terms “energy-saving” and “quiet-running” are becoming very important in the world of variable speed motor drives. Inverter technology is being increasingly accepted and used by a wide range of users in the design of their products.

For low-power motor control, there are increasing demands for compactness, built-in control, and lower overall-cost. An important consideration, in justifying the use of inverters in these applications, is to optimize the total-cost-performance ratio of the drive system.

In order to meet these needs, we have designed and developed a new series of compact, highly functional and very efficient power semiconductor devices called the “SPM (Smart Power Module)”. Fig. 1-(a) shows a real photograph of the SPM. SPM-inverters are a very viable alternative to conventional ones for low-power motor drives due to their attractive characteristics, specifically for appliances such as washing machines, air-conditioners etc. This paper describes in detail the design issues, electrical performance, and other important considerations for designing the system.



(a) Photograph of the SPM

(b) Internal function block diagram

Fig. 1 Photograph of the SPM and the internal function block diagram

II. Description Of Design and Function Features

A. Features

The SPM combines optimized circuit protection and a drive that are matched to the IGBT's switching characteristics. The SPM is composed of three normal IGBTs, three sense IGBTs, three HVICs, one LVIC and one thermistor as shown in Fig. 1-(b). Highly effective short-circuit current detection/protection is achieved through the use of advanced current sensing IGBTs that allow continuous monitoring of the IGBT current. System reliability is further enhanced by the built-in over-temperature and integrated under-voltage lockout protection. The high speed built-in HVIC provides an opto-coupler-less IGBT gate driving capability that further reduces the overall size of the inverter system design. The HVIC facilitates the use of a single-supply drive topology. This allows the SPM to be driven by only one drive supply voltage without a negative bias. The SPM has three divided negative DC terminals to monitor the inverter output current by using three shunt resistors. Nowadays, the sensorless controlled inverter systems are widely used because of the advantages in drive cost, reliability and signal noise immunity. The SPM incorporates these terminals in order to provide a low-cost sensorless control solution [3].

B. Protective functions

The SPM provides two main protective functions. One is control supply under-voltage protection and the other is short-circuit current protection. The principles of operation of these protective functions are described in the timing diagram in Fig. 2. When the control supply voltage drops under its UV detect level, the internal gating signal is blocked and a fault-out signal is generated. Once the supply voltage rises again over the UV reset level, the fault-out signal becomes high and the SPM is operated by the command signals. The LVIC of the SPM detects the low-side collector current level by monitoring the sensing voltage. In the case of a short-circuit, the SPM shuts down the internal gating signal and generates a fault-out signal. This current sensing method provides a simplified and cost-effective solution. The sense-IGBT has very linear sensing characteristics in the range of approximately above 15% of the rated current as shown in Fig. 4. Fig. 5 shows the real sensing voltage waveform. The sensing resistor, R_{sc} , can be selected to determine the trip current level which can be optimized according to the field requirements. Refer to the overall application circuit of Fig. 11, which shows the R_{sc} and R_s parameters related to the short-circuit protection function. Fig. 3 and (1) show the relationship between the sensing resistor R_{sc} and the desired trip current I_{sc} when the shunt resistor R_s is zero.

$$I_{sc} = 82 \times \frac{I_C(\text{Rating Current})}{R_{sc}} \quad (1)$$

DUT: FSAM15SH60

where, I_{sc} : Circuit trip current [A]
 R_{sc} : Sensing resistance [Ω]
 I_C : Rating current of DUT [A]

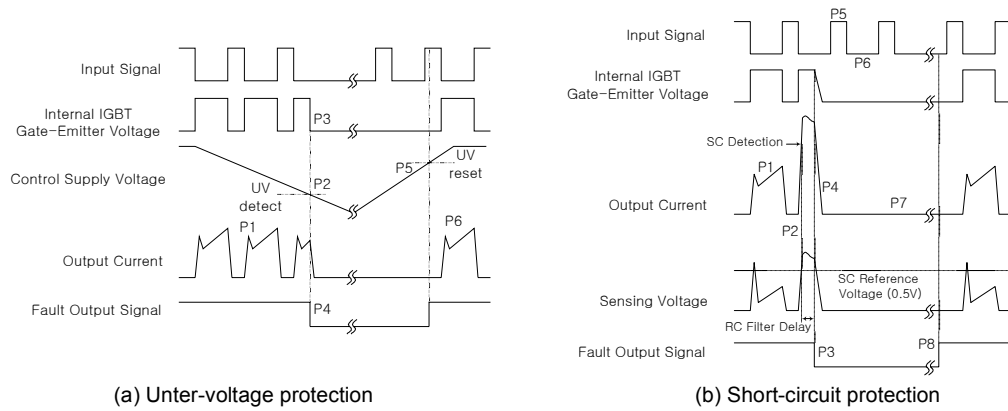


Fig. 2 Time chart of under-voltage and short-circuit protection

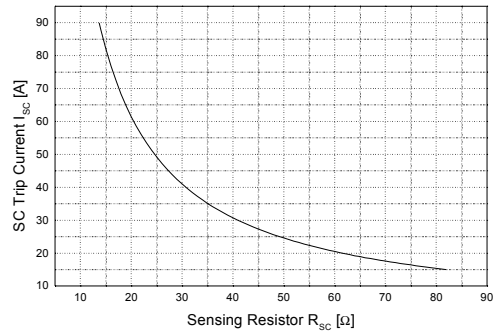


Fig. 3 The relationship between short-circuit trip current (I_{sc}) and sensing resistor (R_{sc})

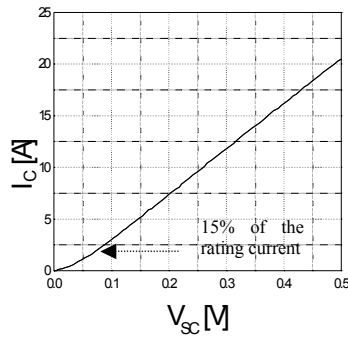


Fig. 4 Sensing characteristics of the sense-IGBT

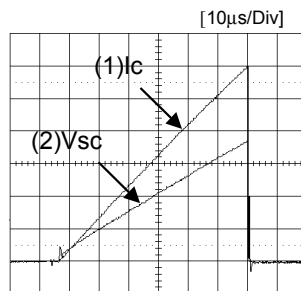


Fig. 5 Measured voltage in the sensing resistor, R_{sc} . Where, (1) Collector current (5A/div.) (2) R_{sc} voltage (0.2/div.)

The circuit trip current, I_{SC} level is in inverse proportion to the R_{SC} value as shown in (1). We can see that the trip current level corresponding to the R_{sc} of 56 is 150% of the rated current. I_{SC} level also decreases along with the increasing of the shunt resistor R_S . In case both R_{sc} and R_s are used, the relationship is shown in Fig. 6. Fig. 7 shows the actual waveforms under a short-circuit protecting situation with $R_s=0\Omega$. The R_{sc} voltage increases as the low-side IGBTs collector current increases. Once the R_{sc} voltage in Fig. 11 reaches to 0.5V, the LVIC shuts down the gating signal after time delay of about $4.5\mu s$, which is mainly caused by a low-pass filter composed of C_{sc} and R_f as shown in Fig. 11. Note that we wanted to detect 150% load current, with R_{sc} of 56Ω , which is around 24A, while using a 15A rated SPM.

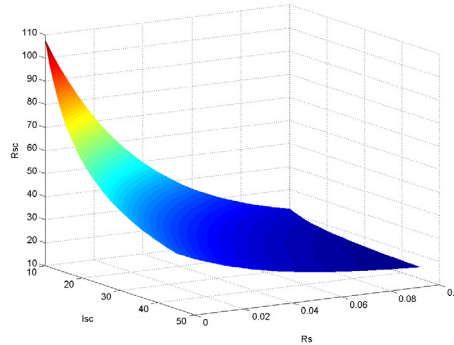


Fig. 6 Short-circuit trip current (I_{SC}) related to sensing resistance (R_{SC}) and shunt resistance (R_S)

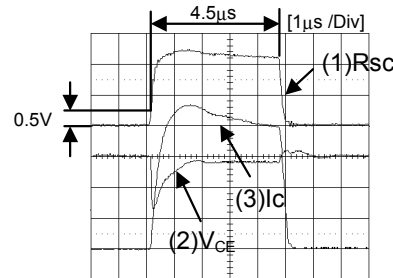


Fig.7 Waveforms for short-circuit protection. Where
 (1) R_{sc} voltage (1V/div.) (2) V_{CE} (100V/div.)
 (3) Collector current (20A/div.)

C. Boot-Strap Circuit

The level-shift feature integrated within the HVIC provides the advantage of an opto-coupler-less control interface for the high-side IGBTs drive. Hence, it is possible to operate all six IGBTs within the SPM using only one drive supply of 15V without a negative bias. To achieve this, some passive components such as capacitors, diodes and resistors should be used externally. The principle of operation of the bootstrap circuit is described in Fig. 8. The voltage source of the bootstrap capacitor is the V_{CC} supply. Its capacitance is determined by the following constraints

- (1) The gate charge required to enhance the IGBT
- (2) I_{QBS} – Quiescent current for the HVIC
- (3) Currents within the level shifter of the HVIC
- (4) Bootstrap capacitor leakage current

Factor 4 is only relevant if the bootstrap capacitor is an electrolytic capacitor. It can be ignored if other types of capacitors are used. Hence, it is always better to use a non-electrolytic capacitor if possible. The following equation describes the minimum charge, that needs to be supplied by the bootstrap capacitor.

$$Q_{BS} \geq 2Q_g + \frac{I_{QBS(max)}}{f} + Q_{Is} + \frac{I_{CBS(leak)}}{f} \quad (2)$$

where, Q_g = Gate charge of the high-side of the IGBT
 f = Switching frequency
 $I_{CBS(leak)}$ = Bootstrap capacitor leakage current
 $I_{QBS(max)}$ = Maximum quiescent current for the HVIC
 Q_{Is} = Level shift charge required per cycle = $5nC$

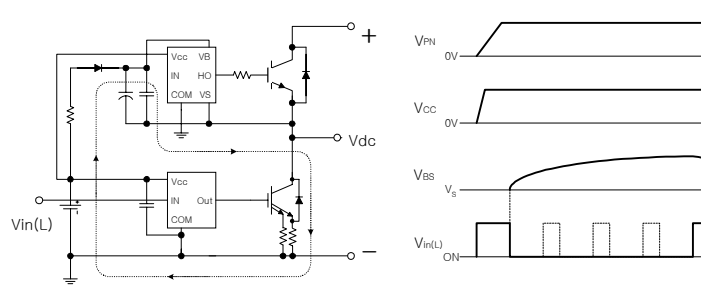


Fig. 8 The bootstrap circuit operation and time chart

The bootstrap capacitor must be able to supply this charge (Q_{BS}), and retain its full voltage. Otherwise, there will be a significant amount of ripple on the V_{BS} voltage, which could fall below the V_{BSUV} (under-voltage detection level). Hence, it is recommended that the charge in the C_{BS} capacitor be at least twice the above value. Due to the nature of the bootstrap circuit operation, a low value capacitor can lead to overcharging, which could in turn damage the HVIC. Hence, to minimize the risk of overcharging and further reduce the ripple on the V_{BS} voltage, it is recommended that the C_{BS} value be multiplied by a factor of 15. The minimum bootstrap capacitor value can be obtained from (3). Note that the following (4) should be used for a specific system application, with an extended period of application of the standstill mode of the PWM output, during the changing of the rotor direction. It can occur in washing machine drive applications where the voltage of V_{BS} can be lowered to an under-voltage protection level.

$$C_{BS} \geq 15 \times \frac{2 \left(2Q_g + \frac{I_{QBS(max)}}{f} + Q_{Is} + \frac{I_{CBS(leak)}}{f} \right)}{\Delta V} \quad (3)$$

where, ΔV = the allowable discharge voltage of the C_{BS} .

$$C_{BS} \geq \frac{I_{QBS(max)} \times \Delta t}{\Delta V} \quad (4)$$

where, Δt = the period of standstill mode and all of the IGBTs are in turn-off state.

The C_{BS} capacitor only charges when the high-side of the device is off and the V_S voltage is pulled down to ground. Therefore, the on-time of the low-side IGBT must be sufficient to ensure that the charge drawn from the C_{BS} capacitor can be fully replenished. Hence, inherently there is a minimum on-time of the low-side IGBT (or off-time of the high-side IGBT).

III. Structure and Packaging

The narrow space multi-die attach technology is used in the SPM. This results in reduced noise, size and less mutual interference. The package is designed to guarantee the best heat transfer from the power chips to the outer heat-sink by using the Ceramic-Pad attaching technology. The ceramic-attached lead frame that includes all the power chips and ICs is transfer molded with good insulation and high conductivity materials. This allows for low cost, high thermal performance. The lead frame structure has a 1mm down-set shape. This makes the thermal resistance low but doesn't reduce the distance between lead frame and the outer heat-sink. More down-set thickness affects the reliability and assembly process. The optimization of the bending depth has been obtained by doing simulations and experimental tests. The total thickness of the molding is 7.2mm and the ceramic thickness is 2mm. Fig. 9 shows the cross sectional structure of the SPM.

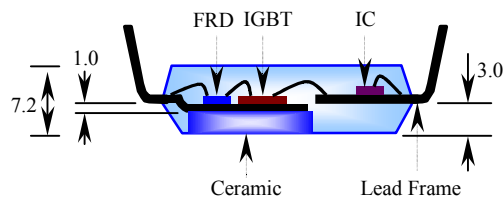


Fig. 9 Cross sectional structure of SPM (unit: mm)

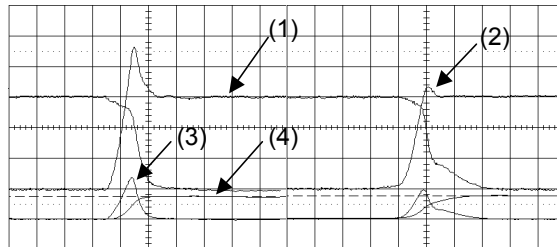
IV. Electrical Characteristics and Performance

A. Electrical Characteristics

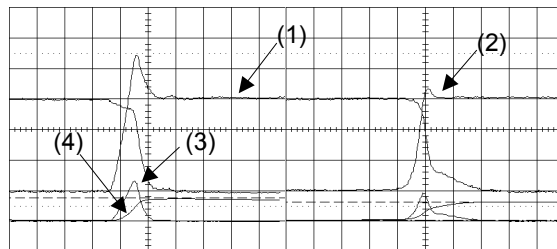
Table 1. shows the basic electrical characteristics of the FSAM15SH60. The table also includes the switching loss data at T_j of 125°C condition. This will be utilized for calculating the SPM power loss. Fig. 10 is the switching waveforms of high-side, low-side IGBTs of the SPM under conditions shown in Table 1.

Table 1: Electrical characteristics of the SPM

Item	Symbol	Condition	Min.	Typ.	Max.	Unit
Collector-emitter Saturation Voltage	$V_{CE(sat)}$	$V_{CC} = V_{BS} = 15V$ $V_{IN} = 0V$	-	-	2.5	V
		$I_C = 15A, T_j = 25^\circ C$	-	-	2.6	V
FWDi Forward Voltage	V_{FM}	$V_{IN} = 5V$	-	-	2.5	V
		$I_C = 15A, T_j = 125^\circ C$	-	-	2.3	V
Switching Times	t_{ON}	$V_{PN} = 300V, V_{CC} = V_{BS} = 15V$ $I_C = 15A, T_j = 25^\circ C$ $V_{IN} = 5V \leftrightarrow 0V$, Inductive Load (High/Low-side)	-	0.34	-	us
	$t_{C(ON)}$		-	0.15	-	us
	t_{OFF}		-	0.58	-	us
	$t_{C(OFF)}$		-	0.25	-	us
Turn-on switching loss	$E_{SW(ON)}$	Same as Switching Times except $T_j = 125^\circ C$	-	0.37	-	mj/pulse
Turn-off switching loss	$E_{SW(OFF)}$		-	0.34	-	mj/pulse
Collector-emitter Leakage Current	I_{CES}	$V_{CE} = V_{CES}, T_j = 25^\circ C$	-	-	250	uA



(a) High-side on/off switching waveform (100ns/div.)



(b) Low-side on/off switching waveform (100ns/div.)

Fig. 10 High/Low side IGBT switching waveforms at $T_j = 25^\circ C$
Where, (1) I_C (5A/div.) (2) V_{CE} (100V/div.)
(3) Switching power loss(4kW/div.)
(4) Switching energy (0.5mjoule/div.)

B. Application Circuit and Design

The circuit configuration for a typical application of the SPM is shown in Fig. 11. A single-supply 15V drives the low-side IGBTs directly and charges the bootstrap circuitry for the HVICs. The LVIC blocks the command signals from the controller and generates a fault signal when a failure mode, the SC current failure or the supply under-voltage failure, is detected. The V_{FO} output is of the open-collector type. This signal line should be pulled up to the positive side of the 5V power supply with approximately $4.7k\Omega$. In the short-circuit protection circuit, the selection of the $R_F C_{SC}$ time constant in the range of $3\sim 4\mu s$ is recommended. R_F should be at least 30 times larger than R_{SC} . The integrated 5V CMOS/TTL compatible Schmitt trigger input conditioning circuit enables direct interface with a microprocessor. The high-side input is pulled up to +5V with a $1.5M\Omega$ resistor and the low-side input is pulled up to V_{CC} with a $100k\Omega$ resistor as shown in Fig. 12. When the driver part of the gate signal is composed of an open-collector, an appropriate pull-up resistor can be selected. When the driver part is composed with push-pull buffer, the low-side pull-up resistor is recommended to be under 2Ω when V_{CC} is +15V. In order to increase the noise immunity, a pull-down capacitor can be used. The capacitances are recommended to be $1.2nF$ for the high-side and $0.47nF$ for the low-side.

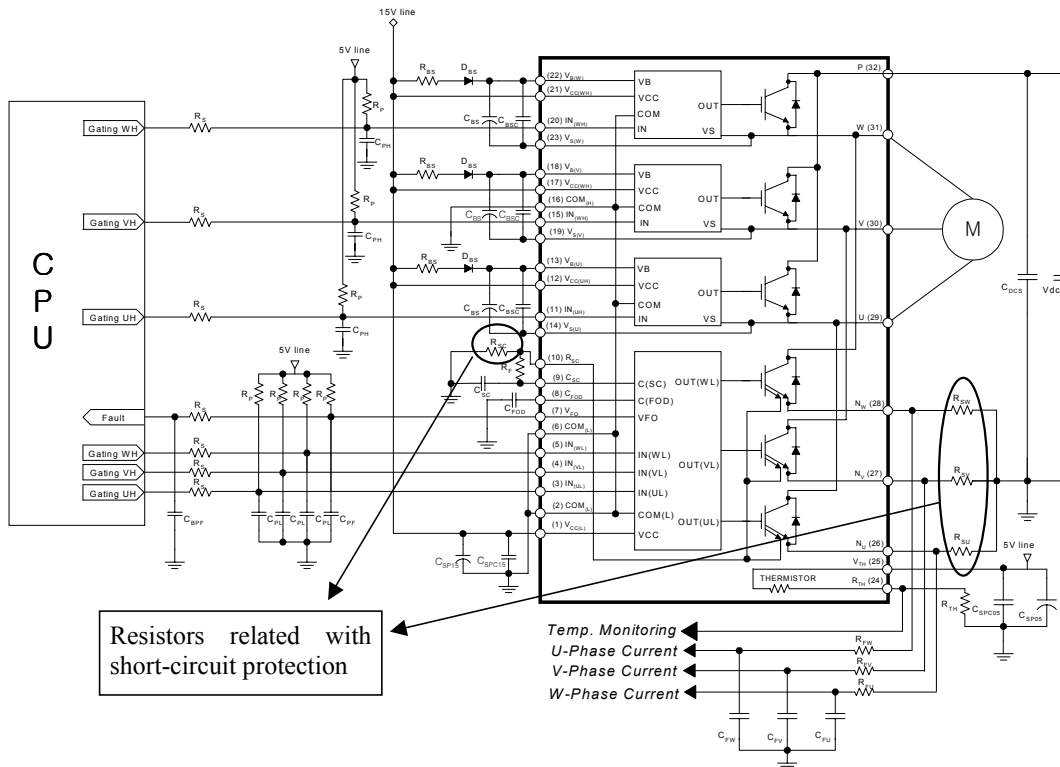


Fig. 11 Typical application circuit example

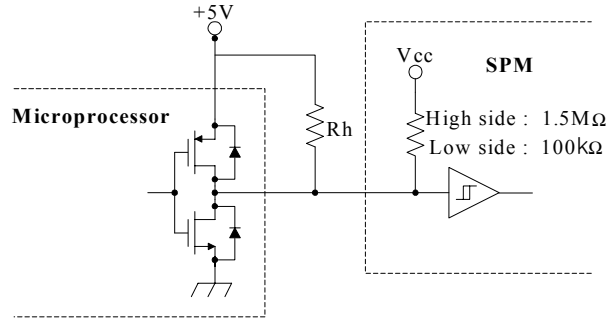


Fig. 12 Example of a pulling-up at a direct connection to a microprocessor

C. Thermal Performance and Operation Ratings

The power carrying potential of a device is dependent on the heat transfer capability of the device. The SPM provides not only good thermal performance but also operating frequency options in accordance with the application.

1. Thermal resistance

For a heat-sink attached device, the major thermal path between its thermal network is the 'junction-to-case-to-heat-sink-to-ambient' path. The junction-to-case thermal resistance $R_{\theta jc}$ is the measurement of heat flow between the chip junction and the surface of the package. $R_{\theta jc}$ can be represented by the following equation.

$$R_{\theta jc} = \frac{T_j - T_c}{P} \quad (5)$$

where, P(W): Power dissipation per device
 T_j (°C): Junction temperature
 T_c (°C): Case reference temperature

Since T_c and P can be measured directly, the only unknown constant is the junction temperature T_j . The Electrical Test Method (ETM) is widely used to measure the junction temperature. The ETM is a test method using the relationship between the junction temperature and the Temperature Sensitive Parameter (TSP). Usually, the thermal characteristics of these parameters are an intrinsic electro-thermal property of semiconductor junctions. For example, the forward-biased voltage drop of a diode and the saturation voltage of an IGBT are such parameters. Once the relationship between T_j and TSP is obtained, the thermal resistance ($R_{\theta jc}$) can be measured. The heating current and TSP-measurement current are alternately applied to the device. The time chart of the duration is shown in Fig. 13. The TSP sampling time must be very short so as not to allow any appreciable cooling of the junction prior to re-applying the heating power. T_j can be obtained in this process using the known relationship between the junction temperature and the TSP. Once T_j reaches thermal equilibrium, its value along with the reference temperature T_c and applied power P is recorded. Using the measured values and (5), the junction-to-case thermal resistance $R_{\theta jc}$ can be estimated. After obtaining $R_{\theta jc}$, it can be used for various thermal analyses. For example, one can predict the junction temperature T_j in a field condition using the following equation

$$T_{j(\text{estimated})} = R_{jc} \times P + T_c \quad (6)$$

It can also be used for calculating the device power loss and for the selection of a heat-sink. From the measurement result, the typical value of the thermal resistance of FSAM15SH60 is 2.0°C/W

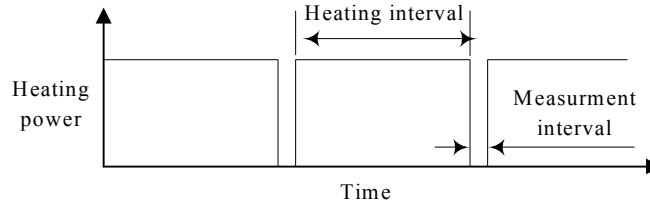


Fig. 13 Thermal resistance test timing chart

2. SPM power losses and ratings

The total power loss in the SPM is composed of conduction and switching losses caused in the IGBTs and FRDs. The loss during the turn-off steady-state can be ignored because it is a very small amount and has little effect on increasing the temperature in the device. The conduction loss depends on the DC electrical characteristics of the device i.e. saturation voltage. Therefore, it is a function of the conduction current and the device's junction temperature. On the other hand, the switching loss is determined by the dynamic characteristics like turn-on/off time and over-voltage/current. Hence, in order to obtain the accurate switching loss, we should consider the DC-link voltage of the SPM system, the applied switching frequency and the power circuit layout in addition to the current and temperature. For the detailed equations for calculating both conduction and switching losses based on a PWM-inverter system for motor control applications, refer to the references [4] and [5].

The typical forward characteristics of an IGBT and a diode can be measured by curve tracer equipment. Assuming that the switching frequency is high, the output current of the inverter can be considered as a sinusoidal one. That is,

$$i = I_{\text{peak}} \cos(\theta - \phi) \quad (7)$$

where ϕ is a phase-angle difference between voltage and current. Using (7), the conduction loss of one IGBT and diode can be obtained. The switching energy loss E_{on} and E_{off} can be measured by the switching waveform of a device. The switching loss depends on the IGBT and diode dynamic characteristics. The turn-off loss depends on the speed of the gate drive and the IGBTs current tail due to the recombination of minority carries. The turn-off energy is measured indirectly by multiplying the current and voltage and integrating them over time. The turn-on loss is due to the rate of current change and the stored charge in the free wheel diode. The loss is measured using the same method. For the calculation of switching loss, the linear dependency of a switching energy loss on the switched current is assumed from the measurement result. The total inverter conduction losses are six times the P_{con} of the IGBT and diode conduction losses. Fig. 14-(a) shows the calculated results including the total power loss due to conduction and switching in the IGBTs and FRDs. The results are obtained by using a high speed SPM device such as the FSAM15SH60. It should be noted that the PWM modulation index $M_I = 0.8$ and $\cos\phi = 0.8$ are used as common parameters in all the calculations. Figs. 14-(a) and 15-(a) show the power losses caused in the SPMs up to a rating current of 15A depending on the rms motor current variation. Fig. 14 shows the SPM power losses and acceptable maximum heatsink temperature to restrict the device's junction temperature below 125°C at 300V of DC-link voltage. Fig. 15 shows a DC-link voltage of 400V. We can see that the difference of about 24% is in the power rating between 15kHz and 3kHz operating conditions. Fig. 16 shows a thermal impedance, which is the thermal resistance between junction and ambient air. The heat-sink used is shown in Fig. 17.

When the DC-link voltage is 300V and I_{rms} is 5A, the IGBT's power loss and FRD's power loss is 4.8W and 1.2W respectively. When thermal impedance is saturated, the difference in temperature of the junction and ambient air is:

$$\Delta T_{IGBT} = Z_{TH_IGBT} \cdot P_{IGBT} = 20 \cdot 4.8 = 96^{\circ}\text{C}$$

$$\Delta T_{FRD} = Z_{TH_FRD} \cdot P_{FRD} = 74 \cdot 1.2 = 88.8^{\circ}\text{C}$$

The junction temperature is:

$$T_{J_IGBT} = \Delta T_{IGBT} + T_{AIR} = 96 + 40 = 136^{\circ}\text{C}$$

$$T_{J_FRD} = \Delta T_{FRD} + T_{AIR} = 88.8 + 40 = 128.8^{\circ}\text{C}$$

The junction temperatures is over 125°C . To keep the junction temperature below 125°C , it must stop operating at full power before around 1000 seconds.

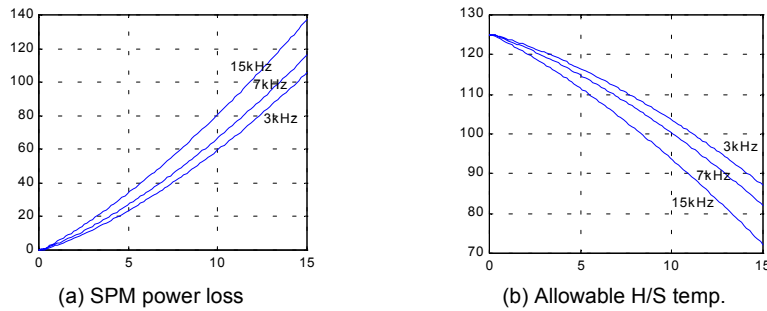


Fig. 14 SPM power losses and allowable H/S temp. at 300Vdc

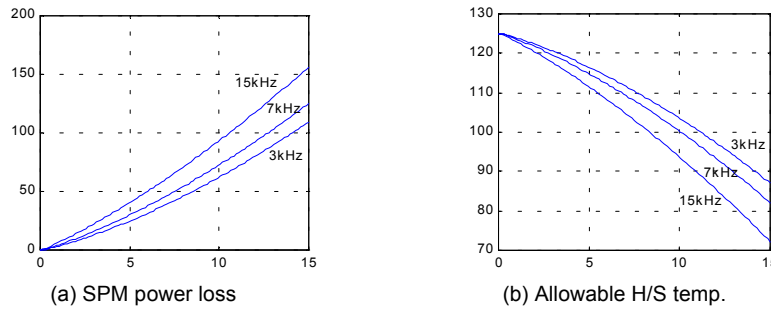


Fig.15 SPM power losses and allowable H/S temp. at 400Vdc

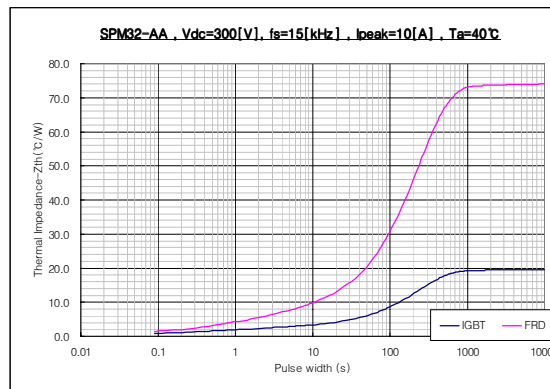


Fig. 16 SPM thermal impedance, junction-to-air

D. Heatsink design guide

The selection of a heat-sink is constrained by many factors including set space, actual operating power dissipation, heat-sink cost, flow condition around a heat-sink, assembly location etc. In this paper, only some of the constraints are analyzed to give some insights in heat-sink selection from a practical application point of view.

Consider the type of heat-sink shown in Fig.17, which can be directly adopted for use in washing machines and modified for use in applications like air conditioners. Figs. 18 and 19 show the analysis results for the heat-sink-to-ambient thermal resistance, $R_{\theta ha}$, in designing the heat-sink. This varies widely with the changes in fin spacing, fin/base-plate length and fin/base-plate width. An increase in fin thickness decreases the total number of fins and the size of the heat-sink, resulting in an increase in thermal resistance.

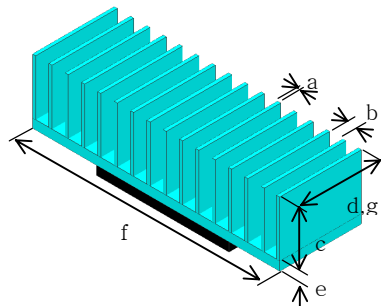


Fig. 17 A heat-sink example
 a=Fin thickness (1.4mm), b=Fin spacing (6.0mm), c=Fin height (25mm)
 d=Fin length (37mm), e=Base-plate thickness (4.0mm)
 f=Base-plate width (112mm), g=Base-plate length (37mm)

Fig. 18 shows the results to see the effect of the base-plate length on thermal resistance. In the case where a cooling fan is not used, we can see that the increase in the length to 150%, that is 55.5mm (37mm \times 1.5), reduces the resistance to 82% (\cong 1.85 $^{\circ}$ C/W), and an increase of 200% (37mm \times =74mm) reduces the resistance to 70.8% (\cong 1.6 $^{\circ}$ C/W). Fig. 19 is the result of the variation in the fin height and it shows that the increase in the height to 150% (25mm \times 1.5=37.5mm) reduces the resistance to 80% (\cong 1.8 $^{\circ}$ c/W). The decrease in the height to 50% (25mm \times 0.5=12.5mm) increases the resistance to 135% (\cong 3.05 $^{\circ}$ C/W). Therefore, increasing the height is more effective reducing the thermal resistance, as compared with increasing the length.

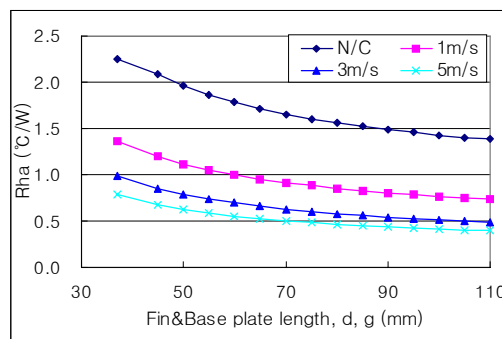


Fig. 18 Analysis results as heat-sink fin & plate length variation

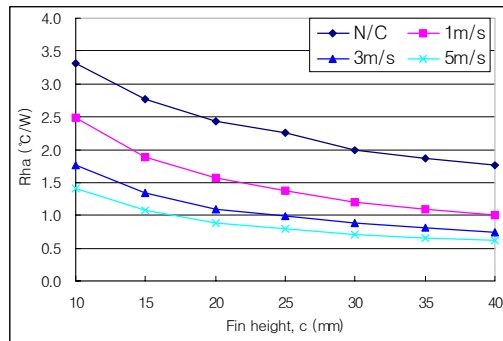


Fig.19 Analysis results as heat-sink fin height variation

V. Conclusion

A novel 3-phase IGBT inverter module, the SPM (Smart Power Module), adopting a new ceramic-based transfer-molding technology, is introduced. Details of the main design concepts, functional capabilities and practical application issues are described. The SPM is targeted at low power inverter applications covering a power rating range up to 3kW at 220Vac input, resulting in smaller system size, higher reliability, and a better cost-performance ratio. With its unique technology, the SPM products will be expanded to cover wider power ranges and applications providing super compact device size in the very near future

References

- [1] T. Yamada et al. "Next Generation Power Module," Intern. Symposium on Power Semiconductor Devices & IC's, Davos, Switzerland, 1994
- [2] Eric R. Mott, John F. Donlon, H. Iwamoto, "New Power Stage Building Blocks for Small Motor Drives," Power Electronics '99 Proceedings, pp.343-349, November, 99
- [3] Nobuyuki Matsui, "Sensorless PM Brushless DC Motor Drives," IEEE Transactions on Industrial Electronics, Vol. IE-43, No. 2, pp. 300-308, 1996, April.
- [4] F. Casanellas, "Losses in PWM inverters using IGBT's," Proc. Inst. Elect. Eng.-Elect. Power Applicat. , vol. 141, no. 5, pp. 235-239, Sept.1994.
- [5] K. Berringer, J. Marvin and P. Perruchoud, "Semiconductor Power Losses in AC inverters," Conf. Rec. of IEEE IAS'95, pp. 882-888, 1995
- [6] Smart power module user's guide, application note AN9018, Fairchild Semiconductor

TRADEMARKS

The following are registered and unregistered trademarks Fairchild Semiconductor owns or is authorized to use and is not intended to be an exhaustive list of all such trademarks.

ACE _x [™]	FAST [®]	MICROWIRE [™]	SILENT SWITCHER [®]	UHC [™]
Bottomless [™]	FAST _r [™]	OPTOLOGIC [®]	SMART START [™]	UltraFET [®]
CoolFET [™]	FRFET [™]	OPTOPLANAR [™]	SPM [™]	VCX [™]
CROSSVOLT [™]	GlobalOptoisolator [™]	PACMAN [™]	STAR*POWER [™]	
DenseTrench [™]	GTO [™]	POP [™]	Stealth [™]	
DOME [™]	HiSeC [™]	Power247 [™]	SuperSOT [™] -3	
EcoSPARK [™]	I ² C [™]	PowerTrench [®]	SuperSOT [™] -6	
E ² CMOS [™]	ISOPLANAR [™]	QFET [™]	SuperSOT [™] -8	
EnSigna [™]	LittleFET [™]	QS [™]	SyncFET [™]	
FACT [™]	MicroFET [™]	QT Optoelectronics [™]	TinyLogic [™]	
FACT Quiet Series [™]	MicroPak [™]	Quiet Series [™]	TruTranslation [™]	

STAR*POWER is used under license

DISCLAIMER

FAIRCHILD SEMICONDUCTOR RESERVES THE RIGHT TO MAKE CHANGES WITHOUT FURTHER NOTICE TO ANY PRODUCTS HEREIN TO IMPROVE RELIABILITY, FUNCTION OR DESIGN. FAIRCHILD DOES NOT ASSUME ANY LIABILITY ARISING OUT OF THE APPLICATION OR USE OF ANY PRODUCT OR CIRCUIT DESCRIBED HEREIN; NEITHER DOES IT CONVEY ANY LICENSE UNDER ITS PATENT RIGHTS, NOR THE RIGHTS OF OTHERS.

LIFE SUPPORT POLICY

FAIRCHILD'S PRODUCTS ARE NOT AUTHORIZED FOR USE AS CRITICAL COMPONENTS IN LIFE SUPPORT DEVICES OR SYSTEMS WITHOUT THE EXPRESS WRITTEN APPROVAL OF FAIRCHILD SEMICONDUCTOR CORPORATION. As used herein:

1. Life support devices or systems are devices or systems which, (a) are intended for surgical implant into the body, or (b) support or sustain life, or (c) whose failure to perform when properly used in accordance with instructions for use provided in the labeling, can be reasonably expected to result in significant injury to the user.
2. A critical component is any component of a life support device or system whose failure to perform can be reasonably expected to cause the failure of the life support device or system, or to affect its safety or effectiveness.

PRODUCT STATUS DEFINITIONS

Definition of Terms

Datasheet Identification	Product Status	Definition
Advance Information	Formative or In Design	This datasheet contains the design specifications for product development. Specifications may change in any manner without notice.
Preliminary	First Production	This datasheet contains preliminary data, and supplementary data will be published at a later date. Fairchild Semiconductor reserves the right to make changes at any time without notice in order to improve design.
No Identification Needed	Full Production	This datasheet contains final specifications. Fairchild Semiconductor reserves the right to make changes at any time without notice in order to improve design.
Obsolete	Not In Production	This datasheet contains specifications on a product that has been discontinued by Fairchild semiconductor. The datasheet is printed for reference information only.